Pharm Res (2017) 34:1956–1969
DOI 10.1007/s11095-017-2207-2

RESEARCH PAPER

Multi-Reservoir Phospholipid Shell Encapsulating Protamine Nanocapsules for Co-Delivery of Letrozole and Celecoxib in Breast Cancer Therapy

Ahmed O. Elzoghby[1,2] • Shaimaa K. Mostafa[1,3] • Maged W. Helmy[1,4] • Maha A. ElDemellawy[5] • Salah A. Sheweita[6]

Received: 5 May 2017 / Accepted: 8 June 2017 / Published online: 22 June 2017

ABSTRACT

Purpose In the current work, we propose a combined delivery nanoplatform for letrozole (LTZ) and celecoxib (CXB).

Methods Multi-reservoir nanocarriers were developed by enveloping protamine nanocapsules (PRM-NCs) within drug-phospholipid complex bilayer.

Results Encapsulation of NCs within phospholipid bilayer was confirmed by both size increase from 109.7 to 179.8 nm and reduction of surface charge from +19.0 to +7.78 mV. The multi-compartmental core-shell structure enabled biphasic CXB release with initial fast release induced by complexation with phospholipid shell followed by prolonged release from oily core. Moreover, phospholipid coating provided protection for cationic PRM-NCs against interaction with RBCs and serum proteins enabling their systemic administration. Pharmacokinetic analysis demonstrated prolonged circulation and delayed clearance of both drugs after intravenous administration into rats. The superior anti-tumor efficacy of multi-reservoir NCs was manifested as powerful cytotoxicity against MCF-7 breast cancer cells and marked reduction in the mammary tumor volume in Ehrlich ascites bearing mice compared with free LTZ-CXB combination. Moreover, the NCs induced apoptotic caspase activation and marked inhibition of aromatase expression and angiogenic marker, VEGF as well as inhibition of both NFκB and TNFα.

Conclusions Multi-reservoir phospholipid shell coating PRM-NCs could serve as a promising nanocarrier for parenteral combined delivery of LTZ and CXB.

KEY WORDS celecoxib · combined delivery · letrozole · multi-reservoir nanocarriers · phospholipid complexation

ABBREVIATIONS

AIs	Aromatase inhibitors
CL	Clearance
CXB	Celecoxib
DMEM	Dulbecco's modified eagle medium
EAT	Ehrlich ascites tumor
EE	Encapsulation efficiency
FBS	Fetal bovine serum
GEN	Genistein
LTZ	Letrozole
$MRT_{0\text{-}inf}$	Mean residence time
MTT	3-(4,5-dimethylthiazolyl-2)-2,5-diphenyltetrazolium bromide
NCs	Nanocapsules
NF-κB	Nuclear Factor Kappa-B
NPH	Neutral protamine Hagedorn
PC	Phosphatidylcholine
PCL	Poly(Caprolactone)
PDI	Polydispersityindex

Electronic supplementary material The online version of this article (doi:10.1007/s11095-017-2207-2) contains supplementary material, which is available to authorized users.

✉ Ahmed O. Elzoghby
ahmed_elzoghby@alexu.edu.eg

1 Cancer Nanotechnology Research Laboratory (CNRL), Faculty of Pharmacy, Alexandria University, Alexandria 21521, Egypt

2 Department of Industrial Pharmacy, Faculty of Pharmacy, Alexandria University, Alexandria 21521, Egypt

3 Department of Pharmaceutics, Faculty of Pharmacy and Drug Manufacturing, Pharos University, Alexandria, Egypt

4 Department of Pharmacology and Toxicology, Faculty of Pharmacy, Damanhour University, Damanhour, Egypt

5 Pharmaceutical and Fermentation Industries Development Center (PFIDC), City for Scientific Research and Tehcnological Aplications (SRTA-City), New Borg El Arab, Alexandria 21934, Egypt

6 Department of Biotechnology, Institute of Graduate Studies and Research, Alexandria University, Alexandria 21526, Egypt

PEG	Poly(ethylene glycol)
PLGA	Poly(lactic-co-glycolic acid)
PS	Particle size
PRM	Protamine
PTX	Paclitaxel
PZI	Protamine zinc insulin
RES	Reticulo-endothelial system
SLS	Sodium lauryl sulphate
TNF-α	Tissue necrosis factor-alpha
VEGF	Vascular endothelial growth factor

INTRODUCTION

Polymeric nanocapsules (NCs) are commonly fabricated from synthetic hydrophobic polymers e.g. PLGA, and PCL via different techniques including nanoprecipitation, emulsion–diffusion, and double emulsification (1). However, synthetic polymers may cause some toxicity or allergic and immunogenic reactions. On the other hand, NCs based on natural hydrophilic polymers e.g. chitosan (2), polyglutamate (3), and polyaspargine (4) were successfully prepared via polymer-coating method. Using this technique, Prego et al. (2) prepared salmon calcitonin-loaded o/w negatively charged nanoemulsion which was then electrostatically coated with a thin layer of positively charged chitosan leading to formation of NCs. Protein and polypeptide nanocarriers have attracted much attention as drug delivery systems in recent years (5–7). Protamine (PRM) consists of polycationic peptides, with nearly 67% of its amino acid composition being arginine (8). PRM has been long used for condensing the spermatid genome and DNA stabilization, as a heparin antagonist, to combine with insulin in formulating PRM zinc insulin (PZI) and neutral PRM Hagedorn (NPH) insulin (9). Moreover, a promising cell-penetratiing potential was reported for low molecular weight PRM (10). Therefore, in our study, we used PRM as an alternative to chitosan for the formation of NCs.

Multi-reservoir nanocarriers were successfully designed with the aim of combined delivery and tailored release of anti-cancer drugs. Drug-phospholipid complexation has been used to enhance the bioavailability of drugs having poor solubility and/or low permeability to biological membranes (11). Mendes et al. (12) developed multi-compartmental PLGA NCs containing paclitaxel (PTX) in its oily core and coated with a phospholipid bilayer entrapping antiangiogenic herbal drug, genistein (GEN). The NCs provided fast release of GEN followed by sustained release of PTX contributing to the enhanced antitumor activity of the nanomedicine.

Estrogens play an essential role in breast cancer development by activating the estrogen receptor. Blocking of estrogen receptor action or estrogen biosynthesis represents promising strategy for treatment of hormone-responsive breast tumors. Aromatase inhibitors (AIs) significantly reduce the production of estrogens in post-menopausal women and hence suppress tumor growth and development (13). LTZ is a potent non-steroidal, third generation AI superior to tamoxifen for the endocrine treatment of estrogen receptor positive breast cancer. However, the poor aqueous solubility of LTZ as well as its systemic adverse effects limits its clinical application. Several delivery systems have been developed to enhance LTZ bioavailability including implants (14), transdermal patch (15), micelles (16), and PLGA nanoparticles (17).

Another obstacle is the development of resistance to AIs, so it is important to develop alternative combination strategies to circumvent or delay the onset of AI resistance (18). Several studies confirmed the beneficial synergistic effect of COX-2 inhibitors (especially CXB) plus AIs in the treatment of breast cancer (19). CXB specifically inhibits COX-2 and has drawn much attention for its anti-cancer properties. Prostaglandin PGE2 formed by COX may enhance the biosynthesis of estrogen by inducing aromatase expression in hormone-dependent breast cancer. Thefore, COX-2 inhibitors impair this sequence and reduce aromatase expression, thus reducing the level of estrogen and breast cancer risk (20). Numerous nanocarriers have been designed to overcome the poor solubility limitations of CXB such as liposomes (21), nanoemulsions (22), and PLGA NPs (23). However, no combined delivery of AI and COX-2 inhibitor in nano-sized formulation was reported till now.

In this study, we have shown that LTZ, a potent AI, can show enhanced anti-tumor activity by encapsulation together with CXB in multi-reservoir nanocarriers. Both LTZ and CXB were entrapped within oily-core PRM-NCs intended to overcome the high lipophilicity of both drugs thus enabling their i.v. administration. To provide biphasic CXB release, CXB was complexed with phospholipid forming a bilayer corona enveloping the NCs. The early CXB released from the outer phospholipid coat will act rapidly to inhibit aromatase expression thus reducing the LTZ dose required to directly inhibit aromatase activity whereas the slowly released CXB from the oily core can offer prolonged enzyme inhibition. We hypothesized that combined delivery of LTZ and CXB via multi-resrvoir NCs would increase their therapeutic efficacy against breast cancer by acting via multiple pathways including dual aromatase inhibition, and potentiation of the anti-tumor efficacy through COX-2 independent mechanisms such as apoptosis induction, inhibition of angiogenesis, and inflammatory mediators such as NF-κB and TNF-α.

MATERIALS AND METHODS

Materials

Letrozole (LTZ) was purchased from Xi'an Natural Field Bio-Technique CO., LTD (China) while Celecoxib (CXB) was

obtained as a gift sample from Amriya Pharmaceutical Industries, PHARCO Corporation (Alexandria, Egypt). Protamine sulfate (PRM), fetal bovine serum (FBS), 3-(4,5-dimethylthiazolyl-2)-2,5-diphenyltetrazolium bromide (MTT), dimethyl sulfoxide (DMSO), ethylene diaminetetraacetic acid (EDTA), Triton X100, Haematoxylin solution, Eosin solution and Canada balsam were purchased from Sigma-Aldrich (St. Louis, USA). Oils (Capryol 90, Capryol PGMC, Lauroglycol 90, labrafac 1349 lipophile and labrafac PG) were kindly supplied by Gattefosse (Lyon, France). Fat-free soybean phospholipids with 75% phosphatidylcholine (Lipoid S75) were kindly provided by Lipoid (Ludwigshafen, Germany). Polyoxyethylene sorbitan monooleate (Tween 80) was purchased from (Riedel-de Häen, Germany). Poly(ethylene glycol) 400 (PEG-400) was supplied by Pharonia Pharmaceuticals Alexandria, Egypt. Sodium lauryl sulphate (SLS) and absolute ethanol were purchased from ADWIC, El-Nasr Pharmaceutical Chemicals Co. (Cairo, Egypt). Methanol HPLC grade was purchased from JT Baker (Phillipsburg, NJ, USA).

Preparation of Multi-Reservoir Dual LTZ-CXB-Loaded PRM-NCs (PC-NCs)

First, two different procedures were explored for preparation of LTZ-loaded PRM-NCs, namely; one- and two-stage mehods (Supplementary Tables S1 & S2). Then, dual LTZ-CXB-loaded oily-core PRM-NCs were prepared by a two-stage polymer-coating technique (24). Briefly, 10 mg of LTZ and 20 mg of CXB were dissolved in 0.75 ml of Lauroglycol® 90 at 50°C then mixed with 10 ml ethanolic solution containing 50 mg Lipoid® S75. This organic solution was poured, under moderate magnetic stirring, into 50 ml of aqueous solution containing Tween® 80 (0.2% *w/v*). A turned milky solution was spontaneously formed as a result of the formation of nanoemulsion due to the diffusion of ethanol towards the aqueous phase. The solvents were then evaporated from NC suspension under reduced pressure in a rotary evaporator (Rotavapor® R-300, Büchi, Switzerland) at 45°C and 50 rpm to a final volume of 10 ml. Finally, 2.5 ml of the nanoemulsion was incubated with 1 ml of 1% *w/v* PRM aqueous solution under gentle magnetic stirring for 30 min leading to the formation of PRM-NCs.

To Elaborate Multi-Reservoir LTZ-CXB-Loaded PRM NCs (PC-NCs)

Film-hydration method was first used for preparation of phosphatidylcholine-CXB complex (12). Briefly, CXB (10 mg) and Lipoid® S75 in 1:2 M ratio were dissolved in 10 ml mixture of chloroform and methanol (1:1 *v*/v) and remained overnight under mild magnetic stirring at room temperature to allow complex formation. A thin film of drug-lipid complex was prepared by the evaporation of the organic solvents in a rotary evaporator at 45°C and 50 rpm. The flask was kept under vacuum for 1 h to ensure complete removal of residual solvent. The phospholipid-drug complex was then used to envelop the dual drug-loaded PRM-NCs where the thin-film was hydrated for 1 h using the dispersion of previously-prepared PRM-NCs containing 10 mg LTZ and 10 mg CXB.

Physicochemical Characterization of NCs

The encapsulation efficiency (EE%) of LTZ and CXB in the NCs was determined indirectly from the difference between the amount of free drug in the supernatant and the total drug amount in the NCs (eq. 1). Free drug content in the supernatant was determined after isolation from the NCs by ultrafiltration-centrifugation (Amicon Ultra-4, 100,000 MWCO, Millipore, Spain) at 3000 rpm for 15 min. Then, samples of the supernatants or the NC suspension (for the total drug content) were dissolved in methanol and analyzed by HPLC.

$$EE\% - \frac{(total\ \ drug) - (free\ \ drug)}{total\ \ drug} \times 100 \quad (1)$$

Particle size (PS) and polydispersityindex (PDI) of dual drug-loaded NCs were measured by photon correlation spectroscopy (PCS) with a NanoZS/ZEN3600 Zetasizer (Malvern Instruments Ltd., UK) (25). The PS was measured with the noninvasive backscattering technology at a detection angle of 173° after dilution with purified water to an appropriate concentration. All of the DLS measurements were performed at 25.0°C for three repeat measurements. For the zeta potential measurement, diluted NC suspension was placed in a universal folded capillary cell equipped with platinum electrodes. The zeta potential values were calculated from the mean electrophoretic mobility, as determined by Laser Doppler Anemometry (LDA).

The *in vitro* release of LTZ and CXB from dual drug-loaded NCs and free drug solution was investigated using dialysis bag method (26). Different NC formulations containing 1 mg LTZ and 2 mg CXB were transferred into dialysis bags (12–14 kDa MWCO VISKING dialysis tubing, SERVA, Germany). The bags were placed into 100 ml of pH 7.4 phosphate buffered saline (PBS) containing 0.5% *w/v* SLS in a shaking water bath at 100 rpm and 37°C. At designated time intervals, 2 ml samples of the release medium were withdrawn followed by compensation with the same volume of fresh release medium. All samples were run in triplicates, filtered through a 0.45 μm membrane filter and the amount of LTZ and CXB released was analyzed by HPLC. The morphology of the dual drug-loaded NCs was examined using Jeol JEM-2100 transmission electron microscope (TEM)

(Tokyo, Japan) at an accelerating voltage of 80 kV (27). A drop of diluted sample was placed on a copper grid, stained with uranyl acetate solution for 30 s and then air-dried before examination.

Colloidal and Lyophilized Powder Stability

The physical stability of the dual drug-loaded NCs was monitored according to time. Therefore, aliquots of the NCs were stored in sealed tubes at 4°C. Particle size, PDI and zeta potential of the NCs were monitored at different time points for a period of 3 months (28). For preparation of lyophilized powdered NCs, 2 ml of the NC suspension containing 5% *w*/*v* mannitol was transferred into 5 ml glass vials and frozen at −80°C then lyophilized using Cryodos-50 freeze-dryer (Telstar, Spain) for 48 h (29). The lyophilized NCs were reconstituted by adding 2 ml of ultrapure water followed by gentle agitation. The reconstituted NCs were evaluated for PS, and PDI. Moreover, the redispersibility index, RI (the ratio between particle size after lyophilization and initial one) and lyophilization yield (% *w*/w) of the NCs were calculated.

Solid State Characterization

To investigate the physical state of LTZ and CXB inside NCs, thermograms of free LTZ, CXB, PRM, CXB-phospholipid complex, blank PRM-NCs, dual drug-loaded PRM-NCs and PC-NCs were recorded by DSC 6 differential scanning calorimeter (Perkin Elmer, USA). Samples were heated in sealed aluminum pans at 10°C/min under nitrogen flow (20 mL/min) in the range of 30–400°C (30). The FTIR spectra of free LTZ, CXB, PRM, blank PRM-NCs, dual drug-loaded PRM-NCs and PC-NCs were recorded using a Spectrum RXI FT-IR spectrometer (Perkin Elmer, USA). Powdered NCs were grounded with KBr and pressed into pellet, and IR transmission spectra were recorded in the range of 4000–500 cm^{-1} [241].

Serum Stability and Hemocompatibility

The dual drug-loaded NCs were incubated at 37°C under mild stirring with an equal volume of 10% FBS for 6 h. At each time interval (0, 1, 2, 4 and 6 h), 50 µL of the mixture was taken then diluted in distilled water (1:50 *v*/v) to be assessed for their PS and PDI using DLS technique. Hemolytic activity was evaluated by determining hemoglobin release from erythrocyte after incubation with the dual drug-loaded NCs (31). Briefly, rat blood samples were collected from retro-orbital plexus into test tubes containing EDTA, centrifuged and washed twice with saline. The obtained RBCs (1 ml) were diluted with saline to 10 ml. 2 ml of the RBCs suspension was incubated with 2 ml of the NC suspension (1 mg/ml) at 37°C with gentle shaking. After 1 h, the samples were centrifuged at 3000 rpm for 5 min. The absorbance (A) of the supernatant was measured by T80 UV/VIS spectrophotometer (PG Instruments Ltd., UK) at 545 nm. A negative control was prepared by mixing 2 ml of the RBC suspension with 2 ml of saline (0% lysis), using 1% Triton X100 as a positive control (100% lysis). The % hemolysis of the samples was calculated as the following equation:

$$Hemolysis\ (\%) = (A_t - A_{nc})/(A_{pc} - A_{nc}) \times 100\% \quad (2)$$

where A_t represents absorbance value of test sample, A_{nc} and A_{pc} stand for absorption value of negative and positive controls, respectively.

In Vitro Cytotoxicity Study

The cell culture experiments were carried out on human breast adenocarcinoma MCF-7 cell line purchased from American Type Culture Collection (ATCC, USA). The cells were maintained in Dulbecco's modified eagle medium (DMEM) containing 10% FBS in a CO_2 incubator (5% CO_2 at 37°C). Cells were seeded at a density of 5×10^3/well in a 96-well plate containing 100 µL of DMEM and allowed to adhere to the plate overnight. The cytotoxicity of the free drug combination and dual-drug loaded multi-reservoir NCs on MCF-7 cells was assessed by the MTT assay (32). Therefore, the medium was replaced by fresh medium containing different concentrations of the drugs either free or encapsulated in NCs and incubated for another 24 h. The culture medium was then replaced with 100 µL of MTT solution (0.5 mg/ml in DMEM) then incubated for further 4 h at 37°C in the dark. After removal of supernatant by centrifugation at 2000 rpm for 10 min, 100 µL of DMSO was added to the wells to dissolve MTT-formazan crystals formed and maintained in agitation for 15 min. Absorbance of the converted dye was measured at a wavelength of 570 nm using a microplate reader (Model 550, Bio-Rad, USA). The relative cell viability was expressed as a percentage of the untreated control wells. The inhibitory concentration (IC_{50}) values were determined using Origin 8.0 (Origin Lab, Northampton, MA) according to the fitted data.

In Vivo Studies

Animals

Pharmacokinetic experiments were performed on female Sprague Dawley rats (200 ± 20 g) housed in stainless steel mesh cages in two groups of six rats each, under standard conditions of light illumination, relative humidity, and temperature. The animals had free access to standard laboratory food and water throughout the study. All procedures were

performed according to a protocol approved by the Animal Care and Use Committee of the Faculty of Pharmacy, Alexandria University, Egypt.

Pharmacokinetic Study

Rats were anesthetized with ether inhalation and injected i.v. with a single dose of free combined LTZ-CXB co-solvent (ethanol:PEG400:Saline 2:3:5 *v*/v) and PC-NCs at a drug dose of 1 mg/kg LTZ and 2 mg/kg CXB. Blood samples (0.5 ml) were collected from the retro-orbital plexus under mild ether anesthesia at designated time intervals (5 and 30 min, 1, 1.5, 2, 4, 6, 8, 12, 24, and 48 h) in EDTA-pretreated tubes. Samples were centrifuged immediately at 5000 rpm for 10 min. The obtained plasma samples were diluted to 2 ml with methanol, vortexed for 10 min, and then centrifuged at 8000 rpm for 20 min (33). A 20 μL amount of the supernatant was injected into the HPLC column to determine the LTZ and CXB plasma concentrations. The different pharmacokinetic parameters were calculated using non-compartmental model with the help of WinNonlin® software, Version 3.0 (Pharsight Corporation Ltd., USA).

Development of Tumor Model

Female BALB/C mice (7–8 weeks of age, about 20–25 g) were housed in a pathogen-free environment at 8 mice/cage. They were supplied with autoclaved and non-fluorescent mouse chow and water. Ehrlich ascites tumor (EAT) cells, supplied from National Institute of Cancer, Egypt, were collected from the ascitic fluid of BALB/c mice harbouring 8–10 days old ascitic tumor. Approximately, 10^7 of EAT cells suspended in PBS were injected subcutaneously into the left side of the mammary fat pad of BALB/c female mice (31). Tumor growth was monitored daily until its volume reached 100 mm^3. Tumor volume was determined by measuring both perpendicular diameters of the tumor using a micrometer according to the following equation:

$$Tumor\ volume = \left(4/3\right) \text{JI}\ (minor\ axis)^2 \text{X}\ major\ axis \qquad (3)$$

In Vivo Anti-Tumor Efficacy

To investigate the *in vivo* anti-tumor efficacy, animals were randomly divided into five groups (8 mice per group). The groups included negative control (healthy mice injected with saline), positive control (inoculated with EAT but untreated), free combined LTZ-CXB solution, dual LTZ-CXB-loaded PC-NCs-treated group; in addition to blank NCs. The tumor-bearing mice were injected i.v. through the tail vein with the free drugs or NCs equivalent to 1 mg/kg LTZ and 2 mg/kg CXB daily for 3 weeks. All the surviving animals were sacrificed after last dose of treatment (i.e. after 21 days). The excised tumors were divided into two parts; one part was used for assessment of tumor growth biomarkers and the second part was used for histopathological studies.

a) Tumor volume

During the treatment period, tumor growth was monitored twice a week. The % increase in tumor volume was calculated for all groups during the treatment. The body weight of each mouse was measured at the initiation of the study and then every week after.

b) Tumor growth biomarkers

Excised tumors were homogenized using cold PBS to make a final 40% tissue homogenate that was divided into 5 aliquots for further quantitative determination of tumor growth biomarkers. Aromatase expression level was quantified using "ARO BioAssay ELISA Kit" (USBiological Life Sciences, USA). Angiogenesis was measured by determination of the level of the angiogenic factor; vascular endothelial growth factor (VEGF) using "VEGF ELISA Kit" (RayBio Tech Inc., USA). Apoptosis induction was measured by determination of tissue caspase 3 level using "Caspase 3 (Casp-3) ELISA Kit" (WKEA Med Supplies Co., USA). Nuclear Factor Kappa-B and tissue necrosis factor-alpha were determined using "BioSource NF-κBp65 ELISA kit" (BioSource International, Inc., USA) and "TNF-α ELISA kit" (RayBio Tech Inc., USA), respectively. All the markers were quantified according to the manufacturer's protocol.

c) Histopathological study

The tumor samples were preserved and fixed in 10% neutral formalin for 24 h at room temperature. A 5 μm thick section were brought down to distilled water, stained with haematoxylin for 5 min and eosin for 2 min, dehydrated in alcohol and mounted in Canada balsam, then examined microscopically. The % necrosis in the excised mammary tumor was assessed semi-quantitatively by examining 10 random sections (×40) from each excised tumor and scored using a scale from 1 to 5. The mean value of all 10 scores was computed for each excised tumor.

Statistical Analysis

Statistical analysis of the *in vitro* and *in vivo* pharmacokinetics results was performed using Student's t-test ($P < 0.05$) (GraphPad Software, Inc., CA, USA). While, IBM SPSS software package (version 20) was utilized to analyze the invivo antitumor activity. For pair-wise comparisons between the

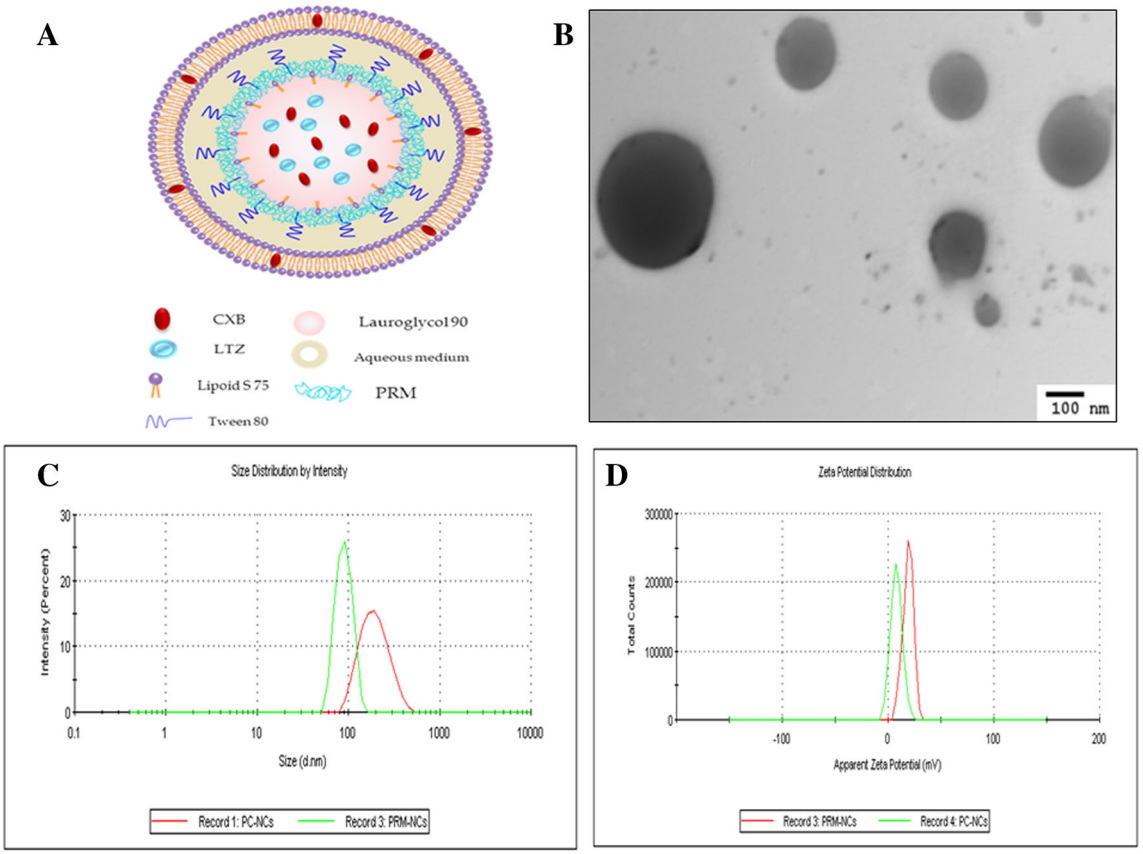

Fig. 1 (**a**) Schematic diagram illustrating the composition of the multi-resrvoir PC-NCs, (**b**) TEM photographs showing morphology of PC-NCs, (**c**) particle size distribution diagrams of PC-NCs and (**d**) their corresponding zeta-potential distribution diagrams.

studied groups, Analysis of Variance test (ANOVA) and Tukey's Multiple Comparison test were used. Significance of the results was judged at the 5% level.

RESULTS AND DISCUSSION

Physicochemical Characteristics of Multi-Reservoir LTZ-CXB-Loaded NCs (PC-NCs)

In this study, multi-reservoir nanocarriers for co-delivery of LTZ and CXB could be developed in two steps. First, LTZ-CXB-loaded PRM-NCs were prepared via polymer-coating method based on o/w spontaneous emulsification process upon mixing of the aqueous phase with a miscible ethanolic oily drug phase followed by electrostatic coating with cationic PRM layer (34). The physicochemical characteristics of both LTZ-loaded PRM-NCs and dual-drug LTZ-CXB loaded PRM-NCs prepared using different variables were discussed in supplementary part (Tables S1-S3 and Figs. S1-S3). In a second step, CXB-phosphatidylcholine (PC) complex was formed then the assembly of the PC envelope surrounding LTZ-CXB-loaded PRM-NCs was accomplished by hydrating the thin phospholipid-drug complex film by the NC dispersion (Fig. 1a) (12). Hydrophilic interactions between the hydrophilic part of the surfactants on the NC surface and the polar head group of the phospholipids may be responsible for this assembly (12,35). The core-shell structure of the multi-reservoir PC-NCs as revealed by TEM confirmed the formation of phospholipid envelope around PRM NCs demonstrating a size of about 200 nm (Fig. 1b). Table I shows the composition and characteristics of LTZ-CXB-loaded PRM-NCs and multi-

Table I Composition and Physicochemical Characteristics of Un-Coated and Multi-Reservoir LTZ-CXB-Loaded PRM-NCs

No.	CXB in oil (mg)	CXB in coat (mg)	S75 in coat (mg)	PS (nm)	PDI	ζ-potential (mV)	LTZ EE (%*w/w*)	CXB EE (%*w/w*)
PRM-NCs	20	–	–	109.7 ± 6.7	0.327 ± 0.007	+19.00	86.36	91.24
PC-NCs	10	10	20	179.8 ± 7.5	0.121 ± 0.01	+7.78	91.50	94.60

*All formulations were prepared with 10 mg LTZ, 0.75 mL Lauroglycol 90, 50 mg Lipoid® S75 in oil, 0.2% (*w/v*) Tween® 80, 1% (*w/v*) PRM solution, 1:2.5 (v:v) PRM:NE

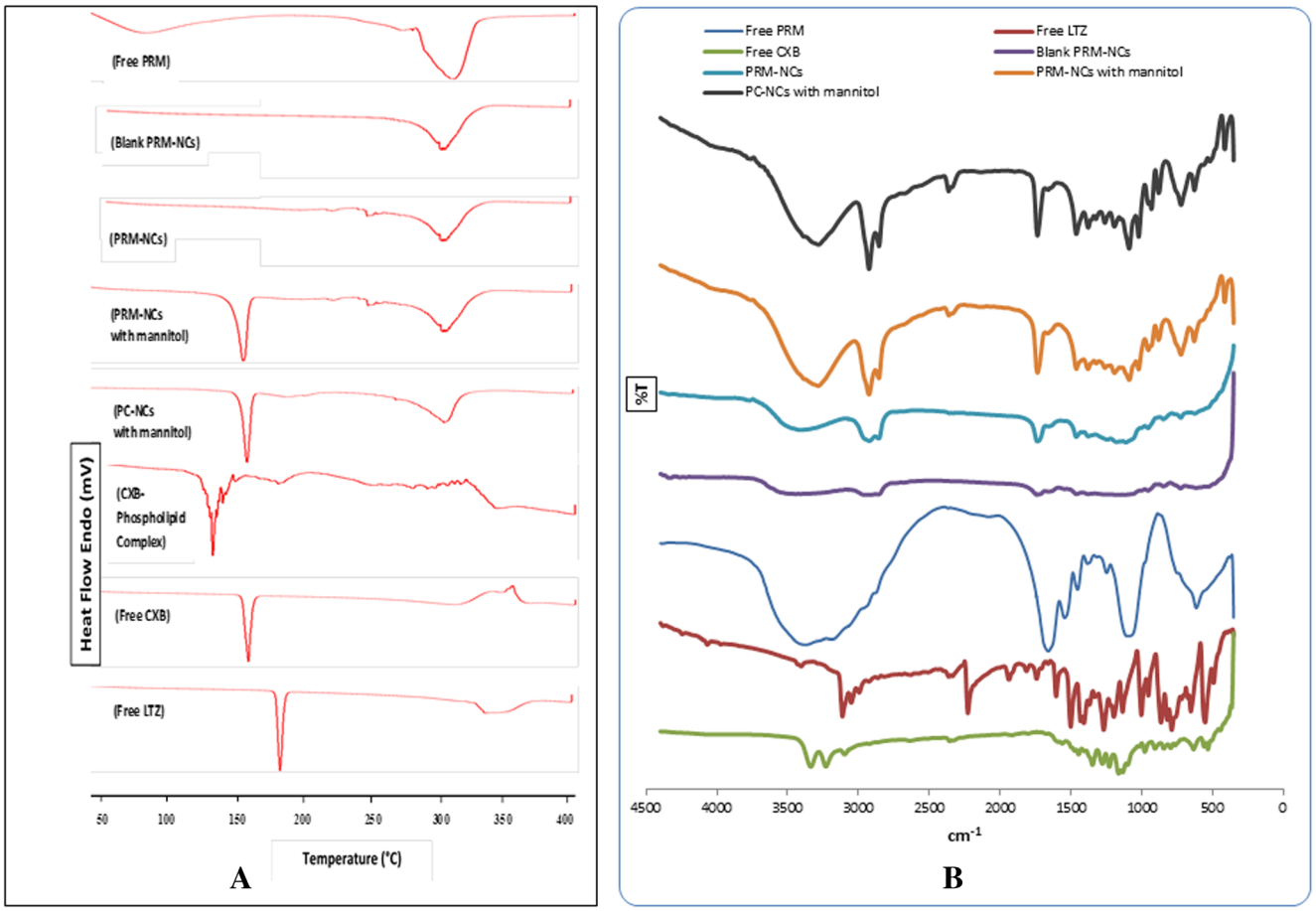

Fig. 2 (**a**) Differential scanning calorimetry (DSC) thermograms and (**b**) FTIR spectra of LTZ, CXB and their developed NCs.

reservoir PC-NCs prepared by two-stage procedure. The size of PRM NCs was remarkably increased upon coating with the phospholipid bilayer from 109.7 to 179.8 nm with a monomodal size distribution (Fig. 1c). Moreover, it was observed that phospholipid bilayer caused a significant reduction of the positive zeta potential of PRM-NCs from +19 mV to +7.78 mV may be explained by the shielding effect of phospholipid shell (Fig. 1d). Similarly, celastrol-loaded MSNs were encapsulated within lipid bilayer containing axetinib using a thin-film hydration technique. Uniform coating of the bilayer was confirmed by both particle size increase from 70 to 120 nm and reversal of the zeta potential from a positive to a detectable neutral charge (35).

Solid State Characterization

The DSC thermograms of free LTZ, free CXB, free PRM and CXB-phospholipid complex were shown in Fig. 2a. The thermogram of free LTZ and CXB showed sharp endothermal peaks at 185 and 165°C corresponding to their melting points, respectively. The DSC thermogram of CXB-phospholipid complex showed the disappearance of the CXB endothermic peak with the appearance of a new peak at 133°C indicating an interaction between CXB and phospholipid thus confirming successful complex formation (36). The thermograms of the two optimized lyophilized NC formulations showed sharp endothermic peak at 165°C corresponding to mannitol melting and the characteristic peak of PRM at 311°C (37). On the other hand, the characteristic endothermal peaks of both drugs have disappeared indicating their amorphization upon encapsulation in NCs (38,39).

The FTIR spectrum of LTZ showed major peaks at 2227.45 cm^{-1} for C ≡ N stretching, 3113.75 cm^{-1} for sp^2 C-H stretching, 690–900 cm^{-1} for out-of-plane CH bending (Fig. 2b) (40). The FTIR spectrum of CXB showed a characteristic S = O symmetric and asymmetric stretching at 1162.03 and 1346.44 cm^{-1}, respectively. Medium intensity bands at 3337.25 and 3231.03 cm^{-1} were seen as a doublet, which are attributed to the N–H stretching vibration of $–SO_2NH_2$ group (41). It can be noted that most of the absorption peaks of LTZ and CXB are still present in the spectra of LTZ-CXB–loaded PRM-NCs & PC-NCs but at lower intensity because of the low drug content. However, the characteristic peak of PRM corresponding to the C = O carbonyl stretching vibrations of amide I band was shifted from 1659.25 cm^{-1} in free PRM spectrum to 1735.69 cm^{-1} in NC specrum (42).

In Vitro Drug Release

Upon encapsulation of oily core PRM-NCs within an envelope of phospholipids, the initial burst release of LTZ from PC-NCs was effectively reduced with 39.56% LTZ was released after 4 h compared to 71.4% LTZ release from un-coated PRM-NCs. This is because LTZ released from the oily core has to diffuse through an additional phospholipid barrier (Fig. 3a). On the contrary, the shell composed of phospholipid-CXB complex coating PRM-NCs could enhance the release of CXB during the initial phase where 25.78% of CXB was released after 4 h compared to only 4.5% from un-coated PRM-NCs (Fig. 3b). Thus, the multi-compartmental system enabled sequential CXB release from the outer phospholipid shell and the oily core consequtively. Complexation with phospholipid enhanced CXB release followed by a phase of sustained release (41.45% after 24 h) by CXB embedded in the oily core. This biphasic pattern of CXB release may be useful where the initially-released fraction can inhibit aromatase expression to reduce the required LTZ dose. The slowly released fraction may act as a depot for prolonged aromatase inhibition. Our findings were in agreement with the previous study of Mendes et al. (12) where genistein was completely released from the phospholipid bilayer encapsulating PLGA oily-core NCs after 48 h whereas only 10% of PTX was released from the core.

Colloidal Stability and Lyophilized Powder Redispersibility

After 3 months storage in the form of colloidal nanosuspension at 4°C, both PRM- and PC-NCs showed PS of 114.5 and 190.67 nm, respectively which are not significantly different from initially stored NCs (109.7 and 179.8 nm) (Fig. 3c). Despite the low value of zeta potential of PC-NCs, their excellent stability may be explained by the surfactant molecules and the stabilizing phospholipid shell (43). Freeze-drying of NCs was reported to increase their stability. Therefore, we have converted our NC suspension into lyophilized powder using mannitol (5% *w/v*) as a

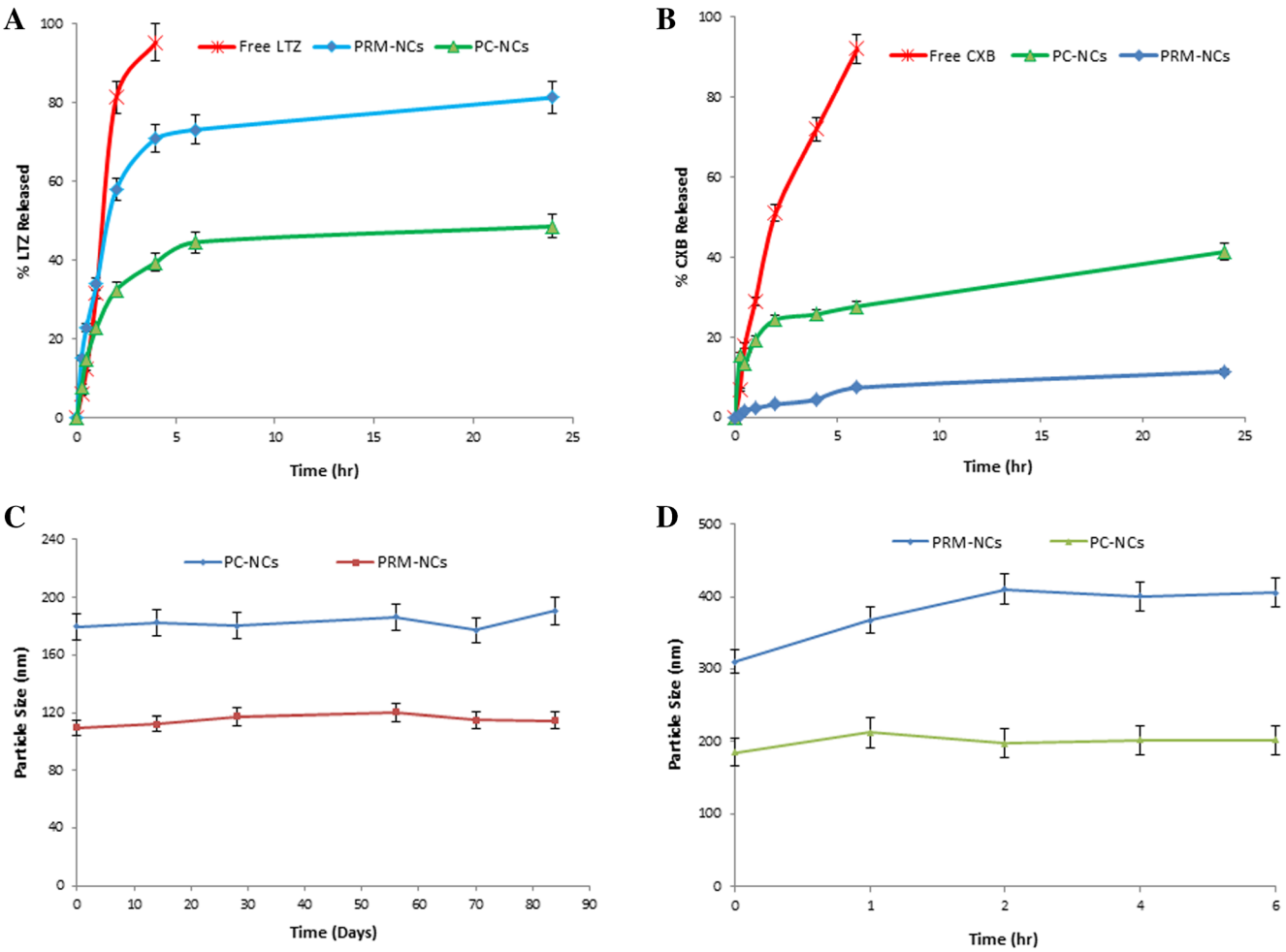

Fig. 3 In-vitro release of (**a**) LTZ and (**b**) CXB from dual drug-loaded PC-NCs compared to free drug solution in phosphate buffered saline (PBS) pH 7.4 containing 0.5% SLS at 100 rpm and 37°C using dialysis bag method. (**c**) Physical stability of the NCs showing particle size change with time and (**d**) Particle size of the NCs after incubation in 10% fetal bovine serum solution for 6 h at 37°C.

Table II Effect of Freeze-Drying on the Particle Size Distribution and Yield of the Optimized LTZ-CXB-Loaded PRM-NCs Formulations

	PS (nm)		PDI	RI (Sf/Si)	Yield (%w/w)
	Before freeze-drying	After freeze-drying			
PRM-NCs	109.7 ± 7.22	115.3 ± 3.81	0.333 ± 0.01	1.05	73.0
PC-NCs	179.8 ± 7.55	200.1 ± 7.28	0.317 ± 0.01	1.11	75.3

cryprotectant. PRM- and PC-NCs could recover their original size after lyophilization with a redispersibility index (RI) of 1.05 and 1.11, respectively (Table II). On the contrary, sticky non-redispersible powder was obtained after lyophilization of NCs in absence of mannitol. Therefore, the presence of cryoprotectant is particularly essential for lyophilization of NCs due to the susceptibility of their oily core to collapse (44).

Serum Stability and Hemocompatibility

After incubation with 10% FBS, PC-NCs could maintain their stability in serum as revealed by no significant size change (201.76 nm) after 6 h (Fig. 3d). This may be attributed to the presence of phospholipid shell inducing steric forces against serum protein interactions. In contrast to PC-NCs, the size of PRM-NCs was instantaneously increased to 310.4 nm once mixed with serum and reached 410.3 nm after 2 h followed a plateau with no significant size change after 6 h. This could be explained by the formation of protein corona arising from binding of negatively-charged serum proteins to the cationic surface of PRM-NCs (31). Consequently, the surface of NCs may be completely occupied with proteins after 2 h resulting in no more increase in their size. As shown in Fig. 4a, PC-NCs demonstrated only 3.7 ± 0.25% hemolysis

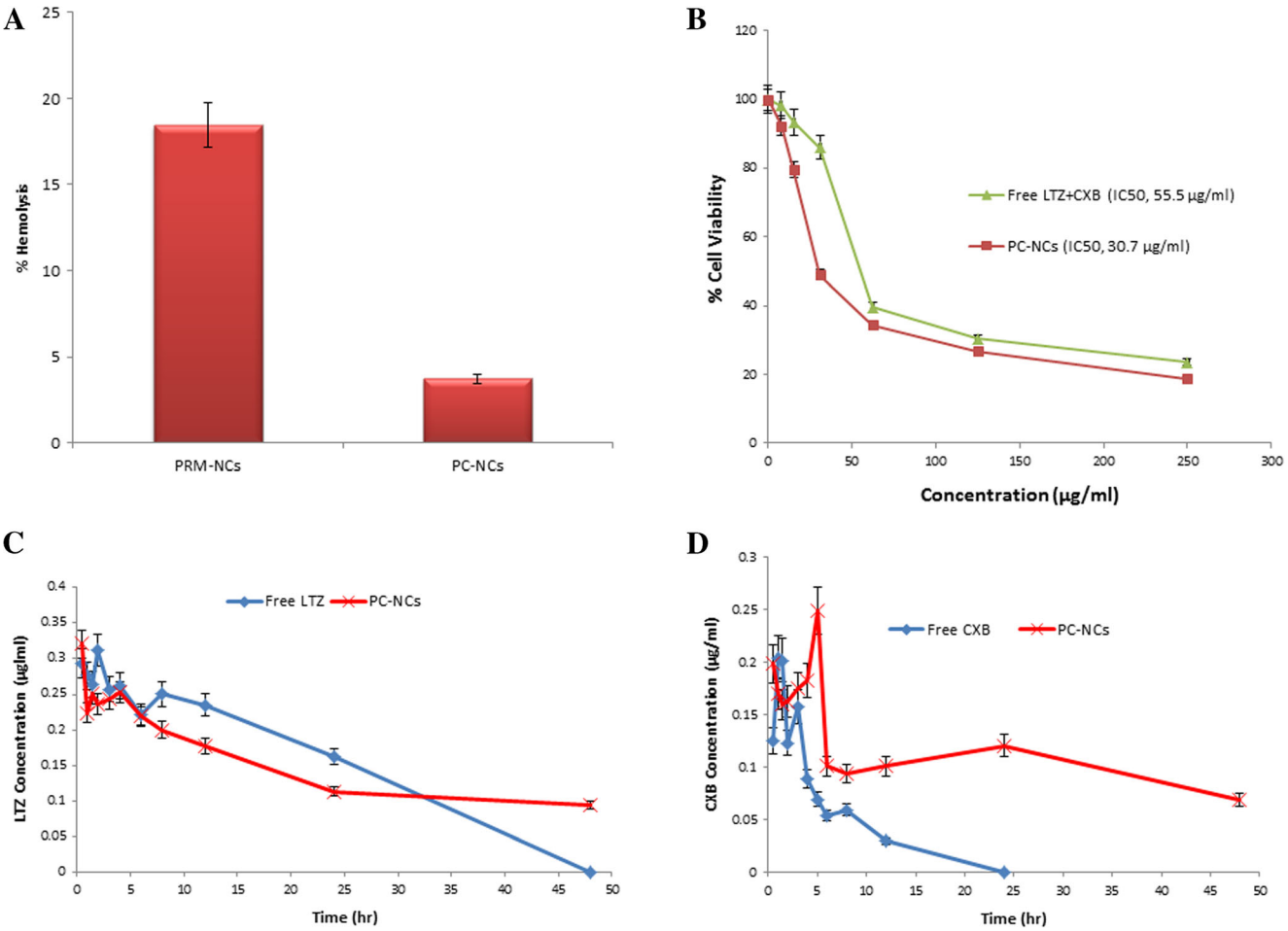

Fig. 4 (**a**) Hemolytic potential of the dual drug-loaded PC-NCs, (**b**) Cytotoxicity analysis of free drugs and dual drug-loaded PC-NCs on MCF-7 breast cancer cells at the concentration of 6–250 µg/ml after 24 h. Data were shown as mean ± S.D. ($n = 3$), $P < 0.05$, Pharmacokinetic analysis showing plasma concentration of (**c**) LTZ and (**d**) CXB from free LTZ-CXB solution and dual drug-loaded PC-NCs following intravenous administration of a single dose of (1 mg/kg LTZ and 2 mg/kg CXB) to healthy female rats, (Mean ± SD, $n = 5$), $P < 0.05$.

Table III Pharmacokinetic Parameters for LTZ from Co-solvent System and PC-NCs After i.v. Injection in Healthy Female Rats

Formula	Free LTZ	PC-NCs
$t_{1/2}$ (hr)	23.45 ± 0.06	29.99 ± 0.07
T_{max} (hr)	0.5 ± 0.001	0.5 ± 0.004
C_{max} (μg/mL)	0.287 ± 0.01	0.32 ± 0.02
AUC $_{0\text{-inf}}$ (μg/mL*hr)	12.32 ± 0.05	10.82 ± 0.12
MRT $_{0\text{-inf}}$ (hr)	35.86 ± 0.10	45.91 ± 0.03
CL (ml/h)	17.45 ± 0.10	18.49 ± 0.11

compared to 18.46 ± 2.32% for un-coated PRM-NCs. This may be attributed to the capping phospholipid shell, as a component of biological membranes, formed a protective cover hindering the interactions between the highly cationic PRM layer at NC surface and the negatively charged membrane of RBCs thus decreasing the hemolytic potential. The hemocompatibility of phospholipid nanoparticles was previously reported where *In vitro* hemolysis test confirmed the safety of the docetaxel-loaded phospholipid nanoparticles for intravenous use (45). Overall, these results confirmed successful assembly of phospholipid bilayer on NCs making them ready for systemic administration with low hemocompatibility in addition to protecting the NCs from opsonization and subsequent clearance by RES.

In Vitro **Cytotoxicity Study**

The cytotoxicity of free LTZ/CXB combination and drug-loaded NCs were assessed on human breast cancer cells, MCF-7, using MTT assay (Fig. 4b). Notably, dual free LTZ/CXB combination and NC dispersions demonstrated considerable reduction in cell viability in a dose-dependent manner. The observed cytotoxic potential of PC-NCs (IC_{50}, 30.7 ± 4.95 μg/ml) was higher than dual free drug combination (IC_{50}, 55.5 ± 2.91 μg/ml) after 24 h incubation period. The superior cytotoxicity of NCs may be explained by the enhanced membrane permeability of NCs via the enveloping phospholipid shell. The unique structural components pf phosphatidylcholine, including a polar head and two non-polar tails, resemble the lipid content of the mammalian cell membrane thus facilitates its penetration (46).

In Vivo **Pharmacokinetics**

In our study, all pharmacokinetic parameters for LTZ and CXB were calculated using non-compartmental model (Tables III and IV). The mean plasma concentration of LTZ and CXB over time for the free drug combination and PC-NCs after i.v. administration into healthy rats is illustrated in Fig. 4c and d. The pharmacokinetic parameters showed that PC-NCs could extend the half-life of LTZ from 24.61 to 29.99 h. Moreover, it was clearly observed that PC-NCs could significantly extend the mean residence time ($MRT_{0\text{-inf}}$) of LTZ from 36.04 to 45.91. As shown in Fig. 4d, PC-NCs exhibited a longer circulation time whereas free CXB was quickly removed from the circulating system after i.v. administration. The mean clearance (CL) value of free CXB was 13-folds greater than PC-NCs. Therefore, the half-life of PC-NCs was significantly higher than free CXB by 14.2-folds. Particles with size below 200 nm can escape clearance by RES resulting in prolonged systemic circulation as compared to those with a larger diameter (47). Therefore, the extended circulation time of our PC-NCs (179.8 nm) may be due to their reduced uptake by RES. The multiple-peak phenomenon of CXB may be explained by the initial release of drug adsorbed on nanocarrier surface followed by the cumulative release of CXB from the core of NCs giving another peak. A similar multiple-peak behavior has also been described in the pharmacokinetic studies of baicalin and chlorogenic acid after their intravenous administration in dogs (48).

In Vivo **Anti-Tumor Efficacy**

Tumor Volume

In the present study, the *in vivo* anti-tumor efficacy of the dual-drug loaded NCs was estimated in Ehrlich Ascites mammary tumor bearing mice. The untreated positive control rats had a progressive increase in tumor volume (740.56 ± 31.6%) after 3 weeks (Fig. 5a). On the other hand, dual-drug loaded PC-NCs exhibithed lower % increase in tumor volume (183.22 ± 11.61%) than combined free LTZ/CXB mixture (314.67 ± 12.2%) ($P < 0.05$). It was reported that aromatase expression and activity are both higher in tumors than in normal breast tissue. The increase in aromatase leads to increase of de novo, local estrogen which stimulate tumor growth and development. The potential benefits of combining AIs and COX-2 inhibitors (CXB) in hormone-sensitive breast cancer therapy were reported (20). In our study, the superior anti-tumor effect demonstrated by our nanovehicular DDS can be attributed to higher intratumoral drug concentration,

Table IV Pharmacokinetic Parameters for CXB from Co-solvent System and PC-NCs After i.v. Injection in Healthy Female Rats

Formula	Free CXB	PC-NCs
$t_{1/2}$ (hr)	4.65 ± 0.04	55.85 ± 0.04
T_{max} (hr)	1.00 ± 0.01	5.00 ± 0.01
C_{max} (μg/mL)	0.18 ± 0.09	0.25 ± 0.01
AUC $_{0\text{-inf}}$ (μg/mL*hr)	1.21 ± 0.02	10.78 ± 0.05
MRT $_{0\text{-inf}}$ (hr)	5.88 ± 0.01	76.20 ± 0.16
CL (ml/h)	359.47 ± 0.09	27.82 ± 0.13

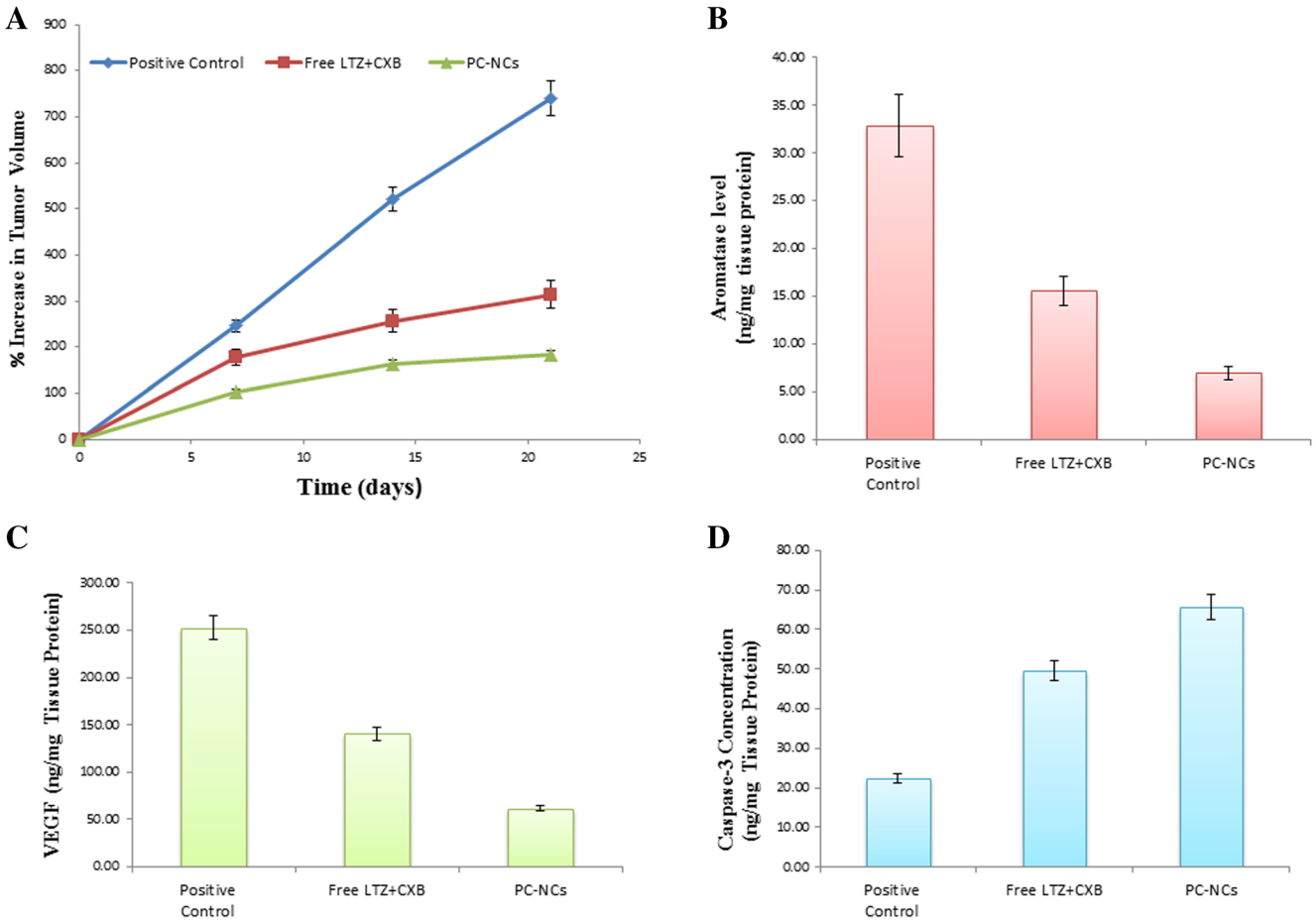

Fig. 5 *In vivo* anti-tumor efficacy showing (**a**) % increase in tumor volume, and the level of the tumor markers including (**b**) Aromatase, (**c**) VEGF-1, and (**d**) Caspase-3 in EAT mice treated for 3 weeks with free drug combination and LTZ-CXB-loaded PC-NCs, compared to untreated positive control.

due to their enhanced accumulation at the tumor site via EPR effect.

Tumor Growth Biomarkers

CXB was reported to exert aromatase-suppressive effects through inhibition of inducible COX-2-dependent pathway in mammary carcinogensis with subsequent inhibition of prostaglandin E2, an activator of aromatase gene expression in mammary tumor (19). Thus, combining AIs plus COX-2 inhibitors may permit a more complete suppression of local estrogen biosynthesis. In our study, a more pronounced inhibitory effect on aromatase level in mammary tumors was achieved by PC-NCs (6.93 ng/mg tissue protein) as compared to free CXB/LTZ combination (15.56 ng/mg tissue protein) ($P < 0.05$) (Fig. 5b). Moreover, PC-NCs showed a marked reduction in the level of VEGF, as one of the most crucial mediators of tumor angiogenesis, from 252.4 ng/mg tissue protein for positive control to 61.33 ng/mg tissue protein compared to free CXB/LTZ combination (140.55 ng/mg tissue protein) ($P < 0.05$) (Fig. 5c). The demonstrated antiangiogenic effect of LTZ and CXB could be attributed to the reduction of estrogen signaling pathways in mammary tumor tissue (49). Several studies have shown that caspase 3 activation is required for apoptosis induction in response to chemotherapeutic drugs. Therefore, defects in apoptosis may cause drug resistance and result in treatment failure. In our study, PC-NCs showed a 2.93 fold elevation in caspase-3 level in mammary tumors relative to positive control group ($P < 0.05$), compared to only 2.21 fold elevation for free LTZ/CXB combination (Fig. 5d). Based on PGE2 inhibition, CXB was reported to modulate survivin and VEGF levels, which are associated to apoptosis evasion, angiogenesis, and proliferation. Thus, CXB can be combined with chemo- or hormonal therapies, for synergistic effects and delayed resistance (49,50).

It is worthy here to mention that CXB has shown anti-tumor efficacy through multiple COX-2 dependent and COX-2-independent mechanisms not related to aromatase function (51). NF-κB inhibition is now considered as a logical therapy for many types of cancer. Moreover, suppression of NF-κB can sensitize tumor cells to chemotherapeutic agents.

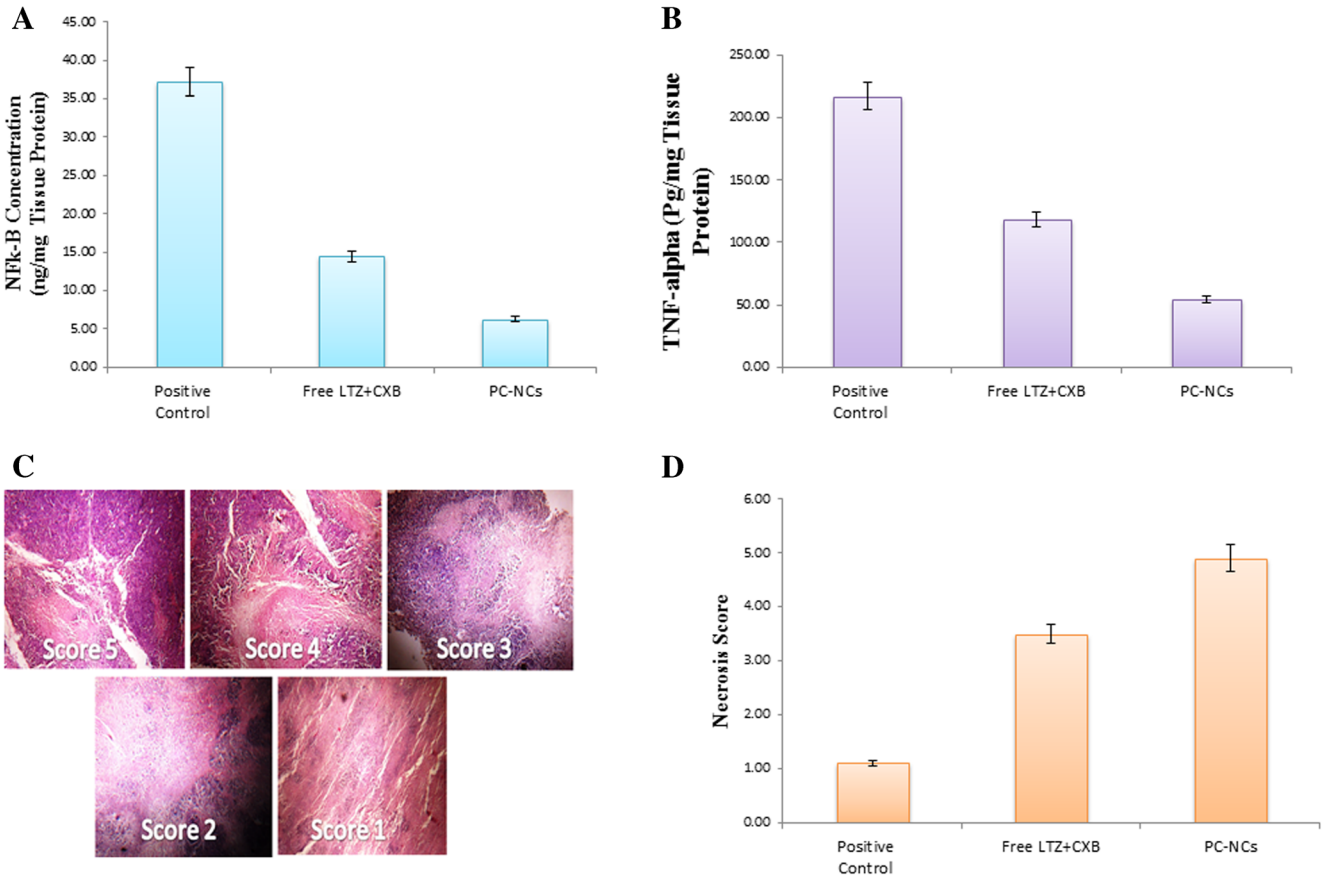

Fig. 6 The level of tumor markers including (**a**) NF-κB and (**b**) TNF-α, (**c**) Scoring of necrosis, and (**d**) Necrotic score in EAT mice treated with free drug combination and dual drug-loaded PC-NCs compared to untreated positive control.

Obviously, the free LTZ/CXB combination succeeded in reducing NF-κB level from 37.26 ng/mg tissue protein for positive control to 14.45 ng/mg tissue protein (Fig. 6a). However, a more pronounced inhibitory effect on NF-κB level was achieved by PC-NCs (6.28 ng/mg tissue protein) ($P < 0.05$). There are growing data to suggest that endogenous TNF-α acts as a tumor promoter which enhances the growth and spread of different tumor types. The most powerful inhibitory effect was achieved by PC-NCs showing a 4-fold reduction of TNF-α level as compared with positive control ($P < 0.05$) (Fig. 6b). On the other hand, free LTZ/CXB combination could also decrease TNF-α level by only 1.8-folds relative to positive control.

Histopathological Study

Histologically, the advantage of nanovehicular delivery systems of LTZ and CXB over the free formula was further confirmed. Fig. 6c shows the scoring system of % necrosis of Ehrlich-induced mammary tumor in mice. It can be noted that PC-NCs showed significantly higher % necrosis than free LTZ/CXB combination (Fig. 6d). The demonstrated increase in necrotic score in the mammary tumor specimens of mice treated with these drugs refers, at least in part, to another add-on mechanism by which the anti-tumor effects were exerted.

CONCLUSION

In this study, we have shown that LTZ, a potent AI, can show enhanced activity by encapsulation with CXB in multi-reservoir PRM-based oily-core nanocapsules (PC-NCs). PC-NCs were developed in the form of phospholipid-CXB complex bilayer enveloping PRM-NCs. A biphasic CXB release and sustained LTZ release could be achieved by PC-NCs rather than PRM-NCs. The NCs were physically stable for three months with no significant changes in their size or zeta potential. The phospholipid bilayer imparted superior hemocompatability and serum stability to the NCs. Moreover, PC-NCs revealed more powerful anti-tumor efficacy compared to PRM-NCs on both breast cancer cells and Ehrlich Ascites tumor-bearing animals manifested by reduction of the tumor volume when compared to free dual drug-treated animals, reduction in the level of aromatase, VEGF, NF-κB and TNF-α and elevation in caspase 3 level. Taken all together, the obtained data confirm the beneficial anti-tumor effects obtained from combining LTZ with CXB in treatment

of breast cancer. Importantly, the nanovehicular delivery of this combination, particularly via multi-reservoir PC-NCs, offers precious anti-tumor effects over the free drugs.

REFERENCES

1. Drozdekand S, Bazylińska U. Biocompatible oil core nanocapsules as potential co-carriers of paclitaxel and fluorescent markers: preparation, characterization, and bioimaging. Colloid Polym Sci. 2016;294:225–37.
2. Prego C, Fabre M, Torres D, Alonso M. Efficacy and mechanism of action of chitosan nanocapsules for oral peptide delivery. Pharm Res. 2006;23:549–56.
3. Abellan-Pose R, Rodríguez-Évora M, Vicente S, Csaba N, Évora C, Alonso MJ, et al. Biodistribution of radiolabeled polyglutamic acid and PEG-polyglutamic acid nanocapsules. Eur J Pharm Biopharm. 2017;112:155–63.
4. Rivera-Rodriguez GR, Lollo G, Montier T, Benoit JP, Passirani C, Alonso MJ, et al. *In vivo* evaluation of poly-l-asparagine nanocapsules as carriers for anti-cancer drug delivery. Int J Pharm. 2013;458:83–9.
5. Elzoghby AO, Hemasa AL, Freag MS. Hybrid protein-inorganic nanoparticles: from tumor-targeted drug delivery to cancer imaging. J Control Release. 2016;243:303–322.
6. Gaber M, Medhat W, Hany M, Saher N, Fang J-Y, Elzoghby A. Protein-lipid nanohybrids as emerging platforms for drug and gene delivery: challenges and outcomes. J Control Release. 2017;254:75-91.
7. Elzoghby AO, Abd-Elwakil MM, Abd-Elsalam K, Elsayed MT, Hashem Y, Mohamed O. Natural Polymeric Nanoparticles for Brain-Targeting: Implications on Drug and Gene Delivery. Curr Pharm Des. 2016;22:3305–23.
8. Yu X, Hou J, Shi Y, Su C, Zhao L. Preparation and characterization of novel chitosan–protamine nanoparticles for nucleus-targeted anticancer drug delivery. Int J Nanomedicine. 2016;11: 6035.
9. Elzoghby AO, Elgohary MM, Kamel NM. Chapter six-implications of protein-and peptide-based nanoparticles as potential vehicles for anticancer drugs. Adv Protein Chem Struct Biol. 2015;98:169–221.
10. Gu G, Xia H, Hu Q, Liu Z, Jiang M, Kang T, et al. PEG-co-PCL nanoparticles modified with MMP-2/9 activatable low molecular weight protamine for enhanced targeted glioblastoma therapy. Biomaterials. 2013;34:196–208.
11. Yu F, Li Y, Chen Q, He Y, Wang H, Yang L, et al. Monodisperse microparticles loaded with the self-assembled berberine-phospholipid complex-based phytosomes for improving oral bioavailability and enhancing hypoglycemic efficiency. Eur J Pharm Biopharm. 2016;103:136–48.
12. Mendes LP, Gaeti MPN, Avila d PHM, Sousa Vieira d M, Santos Rodrigues d B, Ávila Marcelino d RI, et al. Multicompartimental nanoparticles for co-encapsulation and multimodal drug delivery to tumor cells and neovasculature. Pharm Res. 2014;31:1106–19.
13. Kaklamaniand VG, Gradishar WJ. Endocrine therapy in the current management of postmenopausal estrogen receptor-positive metastatic breast cancer. Oncologist. 2017;22:507–517.
14. Ferrati S, Fine D, You J, Rosa d E, Hudson L, Zabre E, et al. Leveraging nanochannels for universal, zero-order drug delivery *in vivo*. J Control Release. 2013;172:1011–9.
15. Li L, Xu X, Fang L, Liu Y, Sun Y, Wang M, et al. The transdermal patches for site-specific delivery of letrozole: a new option for breast cancer therapy. AAPS PharmSciTech. 2010;11:1054–7.
16. Nguyen TL, Nguyen TH, Nguyen CK, Nguyen DH. Redox and pH-responsive poly (amidoamine) dendrimer-heparin conjugates via disulfide linkages for letrozole delivery. Biomed Res Int. 2017;2017:8589212.
17. Nair HB, Huffman S, Veerapaneni P, Kirma NB, Binkley P, Perla RP, et al. Hyaluronic acid-bound letrozole nanoparticles restore sensitivity to letrozole-resistant xenograft tumors in mice. J Nanosci Nanotechnol. 2011;11:3789–99.
18. Hanamuraand T, Hayashi S-I. Overcoming aromatase inhibitor resistance in breast cancer: possible mechanisms and clinical applications. Breast Cancer. 2017;1–13. doi:10.1007/s12282-017-0772-1.
19. Wong TY, Li F, Lin S-M, Chan FL, Chen S, Leung LK. Celecoxib increases miR-222 while deterring aromatase-expressing breast tumor growth in mice. BMC Cancer. 2014;14:426.
20. Prosperiand JR, Robertson FM. Cyclooxygenase-2 directly regulates gene expression of P450 Cyp19 aromatase promoter regions pII, pI. 3 and pI. 7 and estradiol production in human breast tumor cells. Prostaglandins Other Lipid Mediat. 2006;81:55–70.
21. Ju R-J, Zeng F, Liu L, Mu L-M, Xie H-J, Zhao Y, et al. Destruction of vasculogenic mimicry channels by targeting epirubicin plus celecoxib liposomes in treatment of brain glioma. Int J Nanomedicine. 2016;11:1131.
22. Shakeel F, Baboota S, Ahuja A, Ali J, Shafiq S. Celecoxib nanoemulsion: skin permeation mechanism and bioavailability assessment. J Drug Target. 2008;16:733–40.
23. Said-Elbahr R, Nasr M, Alhnan MA, Taha I, Sammour O. Nebulizable colloidal nanoparticles co-encapsulating a COX-2 inhibitor and a herbal compound for treatment of lung cancer. Eur J Pharm Biopharm. 2016;103:1–12.
24. Oyarzun-Ampuero FA, Rivera-Rodríguez GR, Alonso MJ, Torres D. Hyaluronan nanocapsules as a new vehicle for intracellular drug delivery. Eur J Pharm Sci. 2013;49:483–90.
25. Khattab SN, Naim SEA, El-Sayed M, El Bardan AA, Elzoghby AO, Bekhit AA, et al. Design and synthesis of new s-triazine polymers and their application as nanoparticulate drug delivery systems. New J Chem. 2016;40:9565–78.
26. Elgindy N, Elkhodairy K, Molokhia A, ElZoghby A. Biopolymeric nanoparticles for oral protein delivery: design and *in vitro* evaluation. J Nanomed Nanotechnol. 2011;2:1–8.
27. Elzoghby AO, Saad NI, Helmy MW, Samy WM, Elgindy NA. Ionically-crosslinked milk protein nanoparticles as flutamide carriers for effective anticancer activity in prostate cancer-bearing rats. Eur J Pharm Biopharm. 2013;85:444–51.
28. Elzoghby AO, Helmy MW, Samy WM, Elgindy NA. Spray-dried casein-based micelles as a vehicle for solubilization and controlled delivery of flutamide: formulation, characterization, and *in vivo* pharmacokinetics. Eur J Pharm Biopharm. 2013;84:487–96.
29. Elgindy N, Elkhodairy K, Molokhia A, Elzoghby A. Lyophilized flutamide dispersions with polyols and amino acids: preparation and *in vitro* evaluation. Drug Dev Ind Pharm. 2011;37:446–55.
30. Elzoghby AO, Samy WM, Elgindy NA. Novel spray-dried genipin-crosslinked casein nanoparticles for prolonged release of alfuzosin hydrochloride. Pharm Res. 2013;30:512–22.
31. Freag MS, Elnaggar YS, Abdelmonsif DA, Abdallah OY. Layer-by-layer-coated lyotropic liquid crystalline nanoparticles for active tumor targeting of rapamycin. Nanomedicine. 2016;11:2975–96.
32. Freag MS, Elnaggar YS, Abdelmonsif DA, Abdallah OY. Stealth, biocompatible monoolein-based lyotropic liquid crystalline nanoparticles for enhanced aloe-emodin delivery to breast cancer cells: *in vitro* and *in vivo* studies. Int J Nanomedicine. 2016;11:4799.
33. Elzoghby AO, Helmy MW, Samy WM, Elgindy NA. Novel ionically crosslinked casein nanoparticles for flutamide delivery: formulation, characterization, and *in vivo* pharmacokinetics. Int J Nanomedicine. 2013;8:1721.
34. González-Aramundiz JV, Presas E, Dalmau-Mena I, Martínez-Pulgarín S, Alonso C, Escribano JM, et al. Rational design of

protamine nanocapsules as antigen delivery carriers. J Control Release. 2017;245:62–9.
35. Choi JY, Ramasamy T, Kim SY, Kim J, Ku SK, Youn YS, et al. PEGylated lipid bilayer-supported mesoporous silica nanoparticle composite for synergistic co-delivery of axitinib and celastrol in multi-targeted cancer therapy. Acta Biomater. 2016;39:94–105.
36. Freag MS, Elnaggar YS, Abdallah OY. Lyophilized phytosomal nanocarriers as platforms for enhanced diosmin delivery: optimization and ex vivo permeation. Int J Nanomedicine. 2013;8:2385.
37. Awotwe-Otoo D, Agarabi C, Keire D, Lee S, Raw A, Yu L, et al. Physicochemical characterization of complex drug substances: evaluation of structural similarities and differences of protamine sulfate from various sources. AAPS J. 2012;14:619–26.
38. Elgindy N, Elkhodairy K, Molokhia A, Elzoghby A. Lyophilization monophase solution technique for improvement of the physicochemical properties of an anticancer drug, flutamide. Eur J Pharm Biopharm. 2010;74:397–405.
39. Elgindy N, Elkhodairy K, Molokhia A, Elzoghby A. Lyophilization monophase solution technique for preparation of amorphous flutamide dispersions. Drug Dev Ind Pharm. 2011;37:754–64.
40. Dey SK, Mandal B, Bhowmik M, Ghosh LK. Development and *in vitro* evaluation of Letrozole loaded biodegradable nanoparticles for breast cancer therapy. Bra J Pharm Sci. 2009;45:585–91.
41. Chawla G, Gupta P, Thilagavathi R, Chakraborti AK, Bansal AK. Characterization of solid-state forms of celecoxib. Eur J Pharm Sci. 2003;20:305–17.
42. Elzoghby AO, Vranic BZ, Samy WM, Elgindy NA. Swellable floating tablet based on spray-dried casein nanoparticles: near-infrared spectral characterization and floating matrix evaluation. Int J Pharm. 2015;491:113–22.
43. Nerella A, Basava R, Devi A. Formulation, optimization and *in vitro* characterization of letrozole loaded solid lipid nanoparticles. Int J Pharm Sci Drug Res. 2014;6:183–8.
44. Abdelwahed W, Degobert G, Fessi H. A pilot study of freeze drying of poly (epsilon-caprolactone) nanocapsules stabilized by poly (vinyl alcohol): formulation and process optimization. Int J Pharm. 2006;309:178–88.
45. Yadav DK, Pawar H, Wankhade S, Suresh S. Development of novel docetaxel phospholipid nanoparticles for intravenous administration: quality by design approach. AAPS PharmSciTech. 2015;16:855–64.
46. Khan J, Alexander A, Saraf S, Saraf S. Recent advances and future prospects of phyto-phospholipid complexation technique for improving pharmacokinetic profile of plant actives. J Control Release. 2013;168:50–60.
47. Elzoghby AO, Helmy MW, Samy WM, Elgindy NA. Micellar delivery of flutamide via milk protein nanovehicles enhances its antitumor efficacy in androgen-dependent prostate cancer rat model. Pharm Res. 2013;30:2654–63.
48. Li Z, Qju F, Yin X, Zou H, Gong M, Zhai Y, et al. Simultaneous LC-MS/MS quantification and pharmacokinetics of baicalin, chlorogenic acid and forsythin after intravenous administration of Shuang-huang-lian powder to dogs. Anal Methods. 2013;5:2784–92.
49. Rosas C, Sinning M, Ferreira A, Fuenzalida M, Lemus D. Celecoxib decreases growth and angiogenesis and promotes apoptosis in a tumor cell line resistant to chemotherapy. Biol Res. 2014;47:1.
50. Majumder M, Xin X, Liu L, Girish GV, Lala PK. Prostaglandin E2 receptor EP4 as the common target on cancer cells and macrophages to abolish angiogenesis, lymphangiogenesis, metastasis, and stem-like cell functions. Cancer Sci. 2014;105:1142–51.
51. Sareddy GR, Geeviman K, Ramulu C, Babu PP. The nonsteroidal anti-inflammatory drug celecoxib suppresses the growth and induces apoptosis of human glioblastoma cells via the NF-κB pathway. J Neuro-Oncol. 2012;106:99–109.